Theoretical Study of Hydrogen Abstraction and Sulfur Insertion in the Reaction $H_2S + S$

Chenlai (Ryan) Zhou, Karina Sendt,* and Brian S. Haynes

School of Chemical and Biomolecular Engineering, University of Sydney, NSW 2006, Australia

Received: October 30, 2007; In Final Form: January 9, 2008

The reaction of $H_2S + S$ has been characterized at the multireference configuration interaction level with the geometries optimized using the aug-cc-pVTZ basis set and the single-point energy calculated using the aug-cc-pV(Q+d)Z basis set. As in the analogous reaction of $H_2 + S$, the presence of an intersystem crossing enables products (SH + SH) to be formed on the singlet surface through S insertion, which bypasses the triplet barrier (19.1 kJ mol^{-1} relative to SH + SH) of the H abstraction route. This provides theoretical evidence for SH + SH formation without barrier beyond endothermicity at sufficiently low temperatures. The H abstraction route, however, is expected to be competitive at higher temperatures due to a much higher Arrhenius pre-exponential factor (6.9×10^{14} cm^3 mol^{-1} s^{-1} derived from TST calculation) than that of S insertion channel (3.7×10^{13} cm^3 mol^{-1} s^{-1}, derived by a least-squares fit to the measurements). With a slightly higher transition-state barrier than that of the H abstraction channel, the production of $S_2 + H_2$ is less favored due to proceeding via intersystem crossing and insertion. While the formation of HSS + H is energetically unfavorable relative to SH + SH, recombination channels producing H_2SS or the more stable HSSH are expected to occur under collisional stabilization conditions at high pressures.

1. Introduction

It has long since been recognized that the presence of sulfur species in fossil fuels leads to complex chemistry in combustion systems. As noted in a recent review by Schofield,[1] although a satisfactory mechanism has been developed to describe sulfur chemistry as trace species in high-temperature flames, fundamental insight into sulfur behavior at significant concentrations remains elusive.

The kinetics of H_2S thermolysis has been the focus of extensive experimental studies in flow reactors[2−7] and shock tubes[8−13] for decades and has recently been the subject of detailed chemical kinetic modeling studies.[7,14] The unimolecular dissociation channel (R1) was long assumed to be the initiation step in the thermal decompositionof H_2S[8−10] although without theoretical justification

$$H_2S + M \rightarrow SH + H + M \qquad \Delta H_{0K} = 375 \text{ kJ mol}^{-1} \tag{R1}$$

This assumption was however challenged by Woiki and Roth[11] who reported that the rate of atomic S formation was an order of magnitude greater than that of atomic H formation, according to their shock-tube studies. This observation indicates that, due to the possibility of singlet−triplet intersystem crossing, it is not the spin-allowed channel R1 but rather the energetically favored spin-forbidden channel R2 that is responsible for the unimolecular decomposition of H_2S

$$H_2S + M \rightarrow H_2 + S(^3P) + M \qquad \Delta H_{0K} = 291 \text{ kJ mol}^{-1} \tag{R2}$$

The rate expression for R2, based upon the formation profile for atomic S, agreed well with a contemporaneous measurement of H_2S decomposition by Olschewski et al.[12] In addition to the experimental measurements, Olschewski and co-workers[12] reported a crossing energy similar to the endothermicity of R2, based upon a simplified unimolecular rate analysis, the simplifications being necessitated by lack of geometries of crossing intermediates and corresponding potential surfaces.

Recent rate measurements performed by Shiina et al.[13] showed large discrepancies with those obtained by Woiki and Roth[11] and Olschewski et al.,[12] although there was no apparent experimental failure in any of the three studies. Shiina et al.[15] investigated the discrepancy between their rates for R2 and those obtained by Woiki and Roth[11] and Olschewski et al.[12] through measurements of the rate of the reaction, $H_2 + S$. They could find no significant pressure dependence at 900−1050 K and pressures up to 4 bar and concluded that the reverse of R2 must be much slower than the direct abstraction channel to SH + H and hence that the rate of R2 could not be as high as suggested by the earlier investigators.[11,12]

Notwithstanding the differences in the rate, it is significant that all three studies[11−13] revealed a nearly identical activation energy, which was substantially lower than the endothermicity of the bond-cleavage channel R1. As a consequence, Shiina et al.[13] performed quantum chemical calculations to investigate the energy barrier for potential surface crossing in R2. The lowest singlet surface and the three lowest triplet surfaces were calculated at MRCI/cc-pVTZ level of theory, taking the reference energies from state-averaged CASSCF calculations. They reported that the surface crossing energy barrier was 65.4 kJ mol^{-1} higher than the endothermicity of R2 but still 17.4 kJ mol^{-1} lower than the bond dissociation energy of channel R1.

More recently, the reverse channel of R2 was investigated by Maiti et al.[16] who carried out a detailed intersystem crossing study of atomic S insertion using a quantum trajectory surface-hopping method which considered spin−orbit coupling dynam-

* To whom correspondence should be addressed. E-mail: ksendt@chem.eng.usyd.edu.au.

10.1021/jp710488d CCC: $40.75
Published on Web 03/12/2008

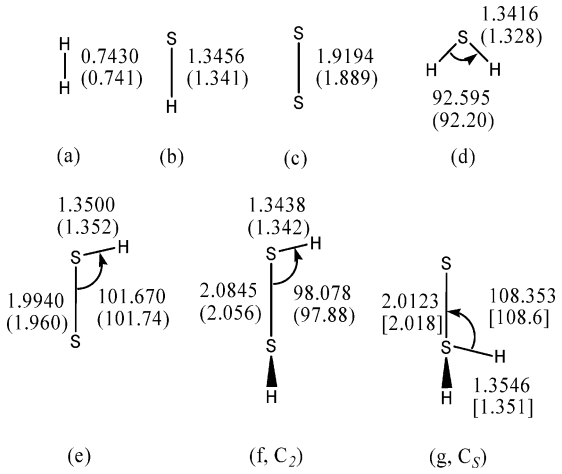

Figure 1. Equilibrium geometry parameters of stable species that were optimized at the MRCI/aug-cc-pVTZ level of theory. Experimental values[31−34] are shown in parentheses ( ), while computed values[25] at MP2/6-311G** level are given in brackets [ ] with bond lengths and angles in angstroms and degrees, respectively. Complete geometry information can be found in the Supporting Information.

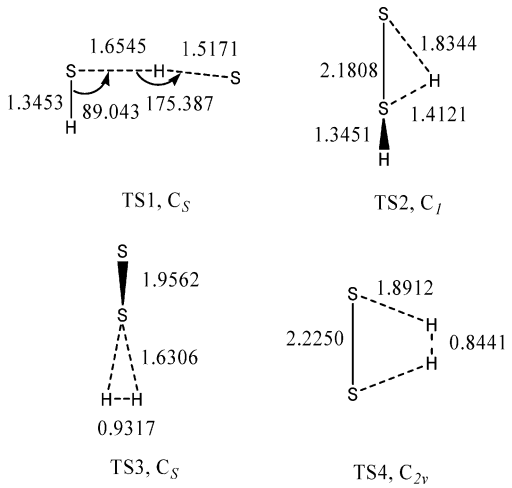

Figure 2. Equilibrium geometry parameters of transition states in the H_2/S_2 system. The transition states were optimized at the MRCI/aug-cc-pVTZ level of theory. Bond lengths and angles are shown in angstroms and degrees, respectively. Complete geometry information can be found in the Supporting Information.

ics. The various reaction channels considered are

$$H_2 + S(^3P) \rightarrow \text{products} \quad \text{(R3)}$$

$$\rightarrow SH + H \quad \Delta H_{0K} = 84 \text{ kJ mol}^{-1} \quad \text{(R3a)}$$

$$\rightarrow H_2S^* \rightarrow SH + H \quad \Delta H_{0K} = 84 \text{ kJ mol}^{-1} \quad \text{(R3b)}$$

$$\rightarrow H_2S \quad \Delta H_{0K} = -291 \text{ kJ mol}^{-1} \quad \text{(R3c)}$$

In agreement with the study of Shiina et al.,[13] the crossing energy, corresponding to the intermediate complex (H_2S^*), is between reactant and product asymptotes of R3. In contrast to the analogous reaction with atomic O, intersystem crossing occurs on the reactant side of channel R3, so bypassing the H abstraction channel (R3a) with its triplet barrier. The relative ease with which system crossing occurs with S is due in part to more significant spin−orbit coupling in S than in O.[16] This study emphasized that the apparent products of the abstraction channel actually arise via the initial intersystem crossing and insertion.

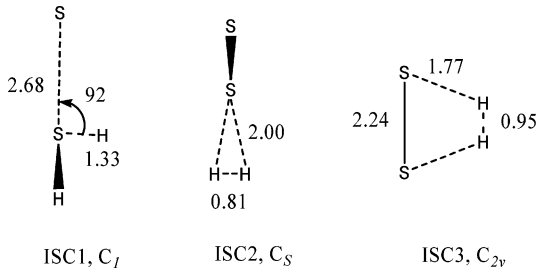

Figure 3. Approximate ISC geometries in the H_2/S_2 system with bond lengths and angles shown in angstroms and degrees, respectively.

The occurrence of intersystem crossing in other reactions of S has also been suspected, for example by Tsuchiya et al.[17] who found no barrier for the reaction of atomic S with a wide range of hydrocarbon species, distinct from the analogous reactions with O, and consistent with the crossing mechanism described above for R3. Similarly, Shiina et al.[13] found reaction R4 to proceed without any barrier beyond its endothermicity and suggested that this might be due to crossing and insertion. This possibility opens up a number of interconnected product channels, some of which have been shown to be important in the overall mechanism of H_2S thermolysis,[7,14] for example

$$H_2S + S(^3P) \rightarrow \text{products} \quad \text{(R4)}$$

$$\rightarrow SH + SH \quad \Delta H_{0K} = 27 \text{ kJ mol}^{-1} \quad \text{(R4a)}$$

$$\rightarrow H_2S_2^* \rightarrow SH + SH \quad \Delta H_{0K} = 27 \text{ kJ mol}^{-1} \quad \text{(R4b)}$$

$$\rightarrow HSSH \quad \Delta H_{0K} = -235 \text{ kJ mol}^{-1} \quad \text{(R4c)}$$

$$\rightarrow H_2SS \quad \Delta H_{0K} = -120 \text{ kJ mol}^{-1} \quad \text{(R4d)}$$

$$\rightarrow HSS + H \quad \Delta H_{0K} = 70 \text{ kJ mol}^{-1} \quad \text{(R4e)}$$

$$\rightarrow H_2 + S_2(^1\Delta_g)$$

$$\rightarrow H_2 + S_2(^3\Sigma_g^-) \quad \Delta H_{0K} = -128 \text{ kJ mol}^{-1} \quad \text{(R4f)}$$

R4a represents H abstraction on the triplet surface, while other possible channels (R4b−R4f), proceeding via the energized complex ($H_2S_2^*$) on the singlet surface, are analogous with R3, due to the possibility of intersystem crossing.

Here it should be noted that Woiki and Roth[11] did find a significant activation barrier for R4, which would appear to argue against the system-crossing channels. However, the use of CS_2 photolysis at 193 nm as the source of S atoms in the Woiki and Roth experiments has been criticized by Shiina et al.,[13] who found photolysis of the coreactant H_2S was also significant at this wavelength. The generation of S atoms by photolysis of COS at 248 nm apparently avoids these problems.[13]

The present study, therefore, aims to elucidate the chemistry of channel R4, using computational chemistry. First of all, the energy barrier of H abstraction on the triplet surface is characterized and the corresponding rate constant evaluated. We then move on to consider the contribution of the spin-forbidden S insertion channels in R4 by means of characterizing the H_2S_2 potential energy surface (PES) at high levels of theory.

2. Computational Methods

Geometry Optimization: Minima and Saddle Points. The equilibrium geometries of stable molecules as well as transition states were optimized at a full valence active space multiref-

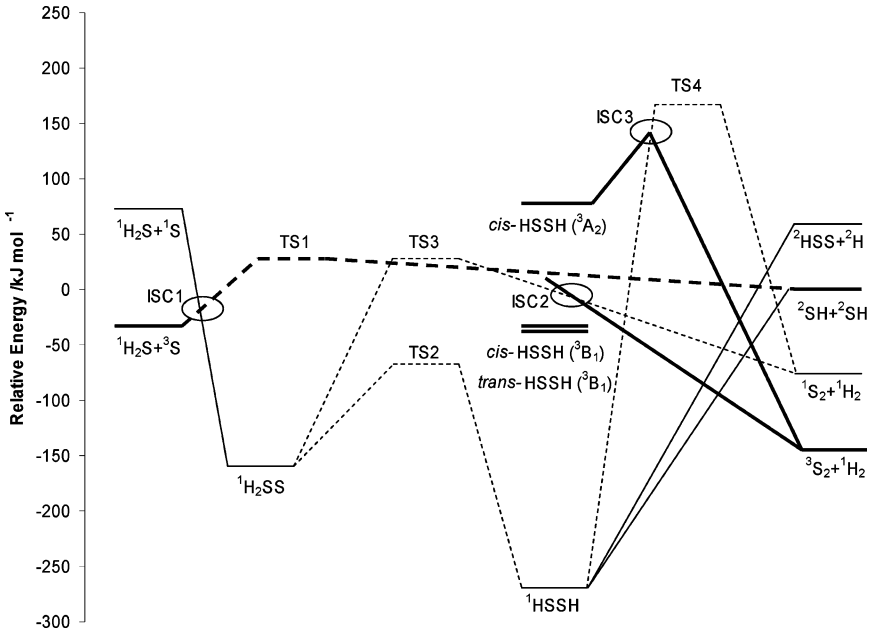

Figure 4. PES for reaction $H_2S + S$: thick lines, triplet surface; thin lines, singlet surface. Energies are shown relative to product set SH + SH calculated at the aug-cc-pV(Q+d)Z level of theory, excluding ZPVE correction. Circles highlight the intersystem crossing energies.

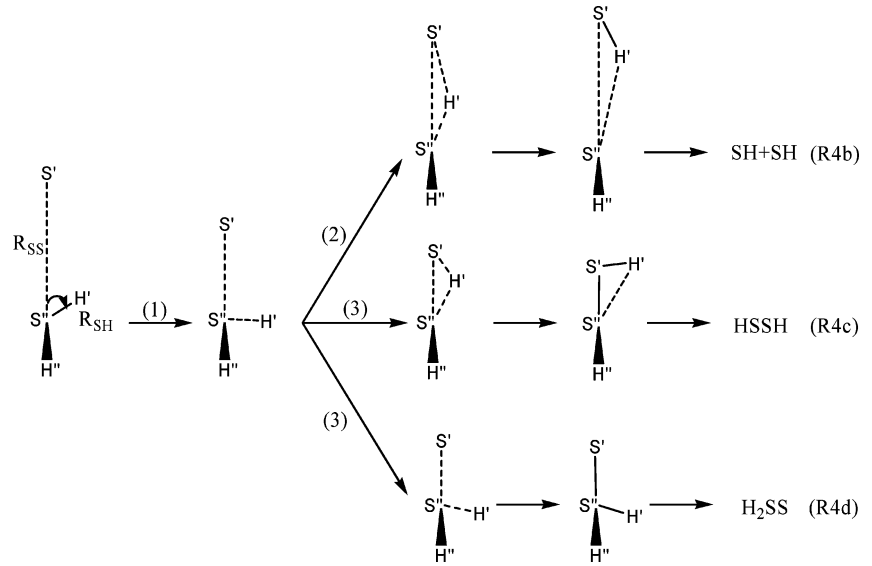

Figure 5. Schematic diagram of atomic S insertion process: (1) A sulfur atom approaches a H_2S molecule on the triplet surface from infinite distance R_{SS} until intersystem crossing occurs. (2) S−S bond remains long in absence of collisional stabilization on singlet surface at low pressure. (3) S−S bond shortens on singlet surface at high pressure due to collisional stabilization.

erence configuration interaction (MRCI) level of theory, using augmented correlation-consistent polarized valence triple-ζ basis set (aug-cc-pVTZ). Subsequently, single-point energy calculations using a higher level basis set were performed at the MRCI/aug-cc-pV(Q+d)Z level of theory with the Davidson correction[18] to approximate the energy of configuration interaction up to quadruple excitations (CISDTQ). The use of the more balanced d-function basis set modified by Dunning et al.[19] is necessary to describe molecules containing second-row atoms. The energy sets of reactants and products were calculated for stable molecules separated by a distance of 50 Å. To reduce the computational expense, vibrational frequencies of stable molecules and transition states were calculated analytically at the CASSCF/aug-cc-pVTZ level of theory using geometries optimized at the CASSCF level. We reported previously that this approximation introduced a discrepancy from MRCI frequency of less than 2%.[20]

PESs: Locating Surface Crossings. To study the possibility of intersystem crossing in atomic S insertion, two-dimensional PES slices were characterized at the MRCI+Davidson/aug-cc-pV(Q+d)Z level of theory, using intermediate geometries partially optimized at MRCI/aug-cc-pVTZ level on both singlet and triplet surfaces. In this way, the intersystem-crossing region was determined, showing the minimum crossing energy on both surfaces.

Detailed geometry parameters are included in the Supporting Information. The quantum chemistry calculations were performed using Molpro,[21] Dalton,[22] and Gaussian 98[23] packages.

3. Results and Discussion

3.1. The PES. Geometry parameters of stable species, transition states, and approximate crossing points involved in R4 are shown in Figure 1, Figure 2, and Figure 3, respectively.

TABLE 1: Electronic Energies, Vibrational Frequencies, and Relative Energies, Including ZPVE Correction of the Optimized Reactants, Products, and Transition States in the H_2/S_2 System

			relative energies (0 K) to SH + SH (kJ mol^{-1})		
species	electronic energies[a] (au.)	vibrational frequencies[b] (cm^{-1})	MRCI[a]	G3	lit. values
$^1H_2$		4225			
$^3S_2$		677			
$^1S_2$		643			
^2SH		2590			
^1H_2S		2628, 2603, 1176			
^2HSS		2483, 908, 549			
^1H2SS	−796.66881903	2701, 2699, 1313, 890, 860, 530	−136.2	−136.7	142.5,[c,f] 146.5[d,f]
^1HSSH	−796.71015887	2558, 2556, 892, 889, 489, 428	−251.8	−252.0	−261.6,[e] −259.5[f]
cis-^3HSSH	−796.62166093	2584, 2580, 266, 189, 94, 62	−31.6		
trans-^3HSSH	−796.62345337	2592, 2591, 371, 296, 258, 82	−33.9		
$^2SH + {}^2SH$	−796.60825787		0	0	0[g]
$^1H_2S + {}^3S$	−796.62103302		−26.2	−23.3	−26.5[h]
$^1H_2S + {}^1S$	−796.57941970		83.1	92.6	
$^2HSS + {}^2H$	−796.58629119		50.3	48.9	43.5[h,i]
$^3S_2 + {}^1H_2$	−796.66301871		−145.4	−152.1	−155.0[h]
$^1S_2 + {}^1H_2$	−796.63787763		−79.7	−85.3	
TS1	−796.59912712	1888,[i] 2575, 873, 386, 287, 245	19.1		
TS2	−796.63490256	1087,[i] 2489, 2110, 988, 744, 398	−60.7		
TS3	−796.59995073	1654,[i] 2026, 1007, 865, 612, 563	21.2		
TS4	−796.54471431	2913,[i] 2031, 998, 514, 463, 353	161.9		

[a] Calculated at the MRCI+Davidson/aug-cc-pV(Q+*d*)Z level of theory. [b] Calculated at the CASSCF/aug-cc-pVTZ level of theory. [c] CCSD(T)/ANO-L calculation, ref 25. [d] CASPT2/ANO-L calculation, ref 25. [e] 0 K value extrapolated from experimental $\Delta H_f°_{298}$, ref 26. [f] CCSD(T)/6-311++G(2df,p)//MP2/6-311++G** calculation, ref 27. [g] Experiment, ref 28. [h] JANAF fourth, ref 29. [i] 0 K value extrapolated from experimental $\Delta H_f°_{298}$, ref 30.

Table 1 lists vibrational frequencies and energies relative to the product asymptote of SH + SH for which the singlet and triplet states are energetically degenerate. A comparison with G3 energies and reported heats of formation of stable species shows that the current computational method has an estimated error of ∼10 kJ mol^{-1}. As depicted in Figure 4, four transition states are characterized at the MRCI level, for the following reactions

$$\text{TS1: } H_2S + S \rightarrow SH + SH$$

$$\text{TS2: } H_2SS \rightarrow HSSH$$

$$\text{TS3: } H_2SS \rightarrow H_2 + S_2(^1\Delta_g)$$

$$\text{TS4: } HSSH \rightarrow H_2 + S_2(^1\Delta_g)$$

In agreement with our earlier study,[14] there are no apparent barriers for the unimolecular dissociation channels of

$$HSSH \rightarrow SH + SH$$

$$HSSH \rightarrow HSS + H$$

Intersystem crossing (ISC1) is found to occur prior to the triplet barrier of TS1 with the minimum crossing energy slightly lower than the SH + SH asymptote. This enables channel R4b to proceed on the singlet surface, bypassing the triplet barrier of R4a. Two other system crossings (ISC2 and ISC3) were identified, but these would appear to be incapable of influencing the kinetics of the overall system: while the singlet−triplet crossing (ISC2) on the product side of TS3 might conceivably affect the S_2 singlet−triplet product distribution, it has no influence on the barrier; the crossing (ISC3) occurring prior to the singlet barrier of TS4 could reduce the barrier, it would have only marginal effect on the reaction rates through this high-energy channel.

3.1.1. Direct Hydrogen Abstraction. With respect to the hydrogen abstraction channel (R4a), we find a substantial energy barrier of ∼45 kJ mol^{-1} above the reactant asymptote of H_2S + S. The high-pressure rate constant has been evaluated based upon TST, including tunneling correction according to Wigner's formulation.[24] By use of a least-squares fit at temperatures ranging from 300 to 3000 K, a three-parameter Arrhenius expression is derived

$$k_{\text{abstraction}} = 3.7 \times 10^6 T^{2.297} \exp(-37.7\ \text{kJmol}^{-1}/RT)\ \text{cm}^3\ \text{mol}^{-1}\ \text{s}^{-1}$$

The tunneling correction is a factor of 2−5 at 300−600 K decreasing to ∼1.3 at 1000 K and ∼1.05 above 2000 K.

3.1.2. Intersystem Crossing in $H_2S + S \rightarrow$ Products. The intermediate geometries arising from insertion of atomic S into H_2S can be considered as a distortion of the H_2SS molecule. As depicted in Figure 5, from the reactant channel (H_2S + S), H′ and S″ initially bond together with a length of R_{SH} when S′ approaches S″ from a distance of R_{SS} on triplet surface. As R_{SS} is reduced to a certain length, interaction between S′ and H′ occurs, forming an intermediate complex with H′ starting to bond with S′. At the same time S′ begins to interact with S″, but in the absence of collisional stabilization, the intermediate complex simply dissociates to products SH + SH (channel R4b; see Figure 5). If the system pressure is sufficiently high so that the S′−S″ bond-forming energy can be effectively removed by collision, stabilized HSSH (R4c) or H_2SS (R4d) molecules are produced.

Migration of H connects the product minima for H_2SS and HSSH on the singlet surface. The saddle point TS2 was optimized to give the geometry shown in Figure 2. The barrier heights of 76 and 191 kJ mol^{-1} (including ZPVE correction) above equilibrium H_2SS and HSSH, respectively, are in good agreement with reported values calculated at CASPT2/ANO-L level.[25]

The PES slices of the S insertion process were characterized in terms of minimizing intermediate complex energies by relaxing the S′−S″−H′ angle θ, for values of R_{SH} and R_{SS} (in the ranges 1.2−2.6 and 2.2−3.6 Å, respectively) separated by 0.2 Å. Meanwhile, the spatial position of the out-of-plane H

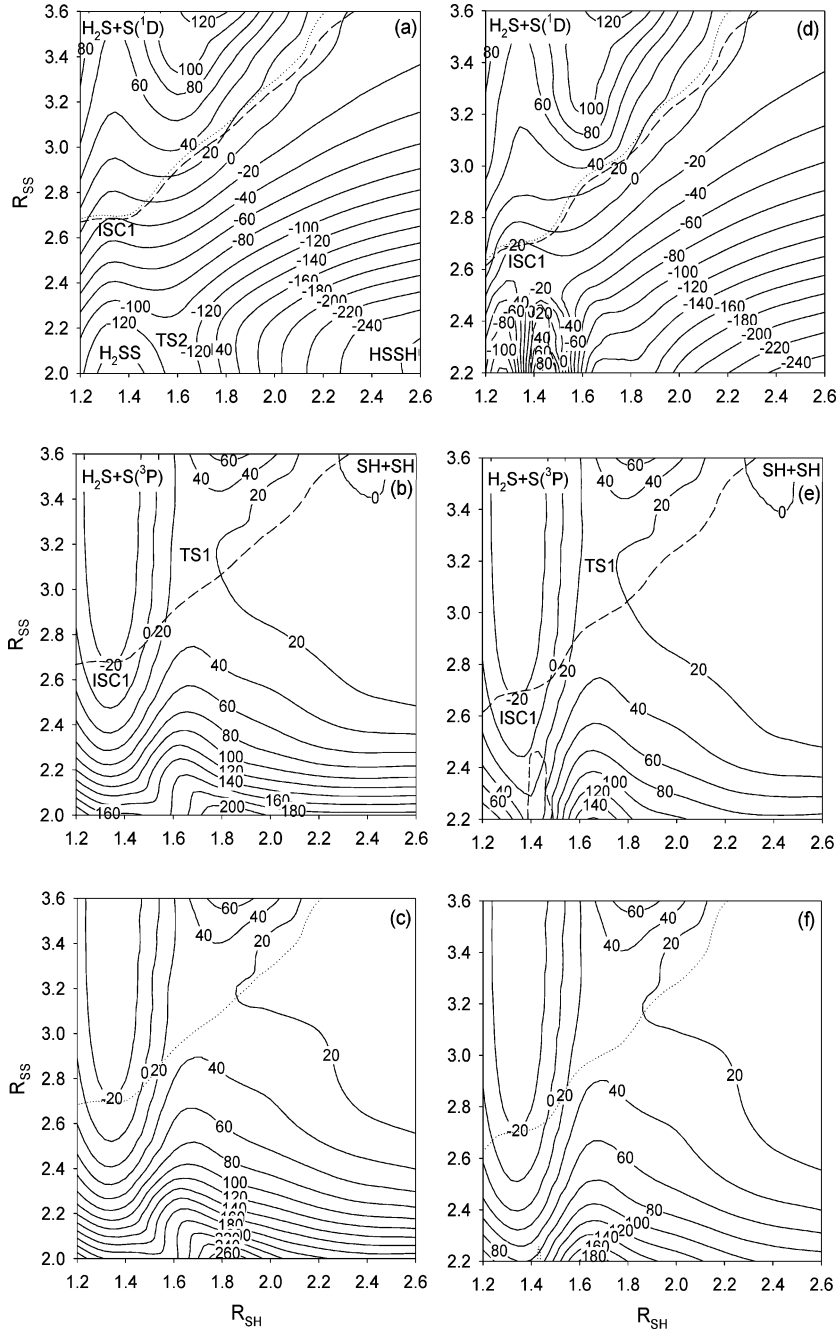

Figure 6. Contour plots of two-dimensional potential energy surfaces. Parts a−c correspond to MRCI+Davidson/aug-cc-pV(Q+*d*)Z energy surfaces of singlet, triplet, and low-lying triplet excited-state, respectively, with geometries optimized on the singlet surface at MRCI/aug-cc-pVTZ level of theory. Parts d−f correspond to MRCI+Davidson/aug-cc-pV(Q+d)Z energy surfaces of singlet, triplet, and low-lying triplet excited-state, respectively, with geometries optimized on the triplet surface at MRCI/aug-cc-pVTZ level of theory. Broken lines and dotted lines denote where singlet−triplet and singlet−excited triplet surface crossing occur, respectively. Energies (in kJ mol^{-1}) are presented as relative energy to product set SH + SH excluding ZPVE correction. Axis units are given in angstroms.

atom, determined by the H″−S″ bond length, the H″−S″−S′ angle, and the dihedral angle relative to the H′−S′−S″ plane, were constrained at the values of equilibrium HSSH species. This simplification is necessary to reduce computational expense without introducing significant extra energy on the partially optimized complex and is justified by the fact that differences in the S−H bond lengths of SH, H_2S, HSSH, and TS1 are within 0.3% (Figure 1). To locate regions of intersystem crossing and their corresponding energies, contour plots of both singlet and triplet two-dimensional PESs are presented in Figure 6, taking R_{SH} and R_{SS} as the two axes. For the singlet-optimized geometries (Figure 6a), the vertical triplet excitation energies (parts b and c of Figure 6) were computed and vice versa for the triplet optimized geometries (i.e., Figure 6e is the triplet-optimized geometry, parts d and f of Figure 6 are the corresponding singlet and low-lying triplet excited-state energies). Furthermore, due to the presence of two degenerate states in each doublet SH species, a combination of two SH species contains up to four states with similar energies on the triplet surface. These were computed using a state-averaged CASSCF wavefunction. In this study, only the two lowest triplet states are shown, corresponding to the ground state (parts b and e of Figure 6) and the low-lying excited state (parts c and f of Figure 6). The energy values shown on the plots are relative to the asymptote of SH + SH (excluding ZPVE correction). The sets of PES slices optimized on the triplet surface show similar

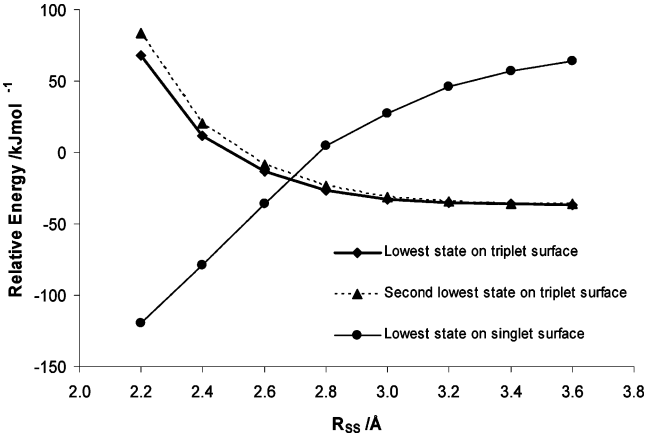

Figure 7. Intermediate energies relative to SH+SH calculated at MRCI+Davidson/aug-cc-pV(5+*d*)Z level of theory, based upon geometries optimized on triplet surface at MRCI/aug-cc-pVTZ level with R_{SH} constrained at 1.3 Å.

patterns to their corresponding optimizations on the singlet surface. This indicates that there are no substantial geometry variations, except for large differences in the region when R_{SS} equals 2.2 and 2.4 Å, while R_{SH} equals 1.4 Å. These are quite compressed geometries with normal optimized angles (104.62° and 99.82°) on the singlet surface (Figure 6a), but they approach linear geometry (175.80 and 155.08°) on the triplet surface (Figure 6e), leading to the high vertical excitation energy from the optimized triplet surface to the corresponding singlet state (Figure 6d).

On each contour plot in Figure 6, the upper-left, upper-right, lower-left, and lower-right corners represent the stable species sets H_2S + S, SH + SH, H_2SS, and HSSH, respectively. The saddle point regions (TS2 corresponding to the transition state for H migration on the singlet surface and TS1 corresponding to H abstraction on the triplet surface) appear around 1.6 Å for in plane S′−H′ bond length (R_{SH}) and 2.1 and 3.2 Å for in-plane S′−S″ bond length (R_{SS}) respectively, in reasonable agreement with the equilibrium geometries of these transition states shown in Figure 2.

According to the PES slices in Figure 6, as the S atom approaches H_2S from infinite distance on the ground-state triplet surface, intersystem crossing is found to occur at R_{SS} around 2.7 Å, producing an excited singlet H_2SS^* with the crossing energy ∼20 kJ mol^{-1} below the threshold of dissociation producing SH + SH but ∼116 and ∼232 kJ mol^{-1} above that of equilibrium H_2SS and HSSH, respectively. The crossing energy from the low-lying excited triplet state is higher than that of the ground-state crossing by ∼5 kJ mol^{-1}. Subsequently, on the singlet surface, the trajectories can skirt around the triplet H abstraction transition state, which has an energy ∼39 kJ mol^{-1} higher. As a consequence, SH + SH is anticipated to be produced without barrier above endothermicity at low pressures while HSSH, which is 116 kJ mol^{-1} more stable than H_2SS, dominates under collisional stabilization conditions at high pressures.

In the crossing region of interest (R_{SH} = 1.3 Å), additional intermediate geometries were optimized on the triplet surface at the MRCI/aug-cc-pVTZ level of theory, and further single-point MRCI energy profiles were calculated using the higher level basis set of aug-cc-pV(5+d)Z. Figure 7 shows the crossing energy of ∼20 kJ mol^{-1} below SH + SH, which is in good agreement with that calculated using a lower-level basis set, proving the suitability of aug-cc-pV(Q+d)Z basis set to describe the PES.

3.1.3. Intersystem Crossing in Channel $H_2SS \rightarrow H_2 + S_2(^3\Sigma_g^-)$. The saddle point corresponding to TS3 (geometry shown in Figure 2) that connects the minima H_2SS and $S_2(^1\Delta_g)$ + H_2 was optimized at the MRCI level on the singlet surface, yielding an energy of ∼21 kJ mol^{-1} higher than asymptote of SH + SH. Further effort was devoted to studying the possibility of reducing the singlet barrier through intersystem crossing in a manner analogous to the S insertion channel (R3c) discussed above. Figure 8 presents the singlet and triplet PESs for the C_s approach of one S atom of S_2 to H_2 with the S atom out of H−S−H plane constrained at the geometry of H_2SS. It is apparent that the intersystem crossing occurs on the product side with the minimum crossing energy of ∼30 kJ mol^{-1} lower than the barrier on singlet surface. This offers the possibility of producing the more stable $S_2(^3\Sigma_g^-)$ molecule directly but does not alter the fact that production of S_2 + H_2 from H_2SS dissociation can only occur with a substantial energy barrier, at least 157 kJ mol^{-1} which is still higher than SH + SH.

3.1.4. Intersystem Crossing in Channel $HSSH \rightarrow H_2 + S_2(^3\Sigma_g^-)$. Another possible channel to produce S_2 + H_2, via direct dissociation of HSSH, was studied at the MRCI level. A substantial barrier (414 kJ mol^{-1} above equilibrium HSSH) is found for the transition state TS4 with C_{2v} symmetry on the singlet surface (geometry shown in Figure 2). To investigate the possibility of intersystem crossing, both planar cis and trans isomers for triplet HSSH were optimized at the MRCI level

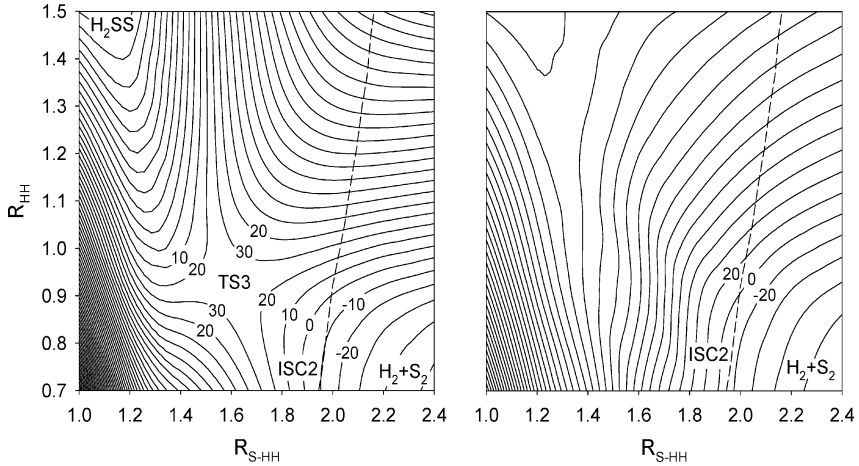

Figure 8. Contour plots of two-dimensional PESs (left, singlet; right, triplet) calculated at MRCI+Davidson/aug-cc-pV(Q+d)Z level of theory. Broken lines denote where intersystem crossing occurs. Energies (in kJ mol^{-1}) are relative to SH + SH. R_{HH} and R_{S-HH} (in angstroms) represent the distance between two H atoms and the distance between one S atom and the center of two H atoms, respectively.

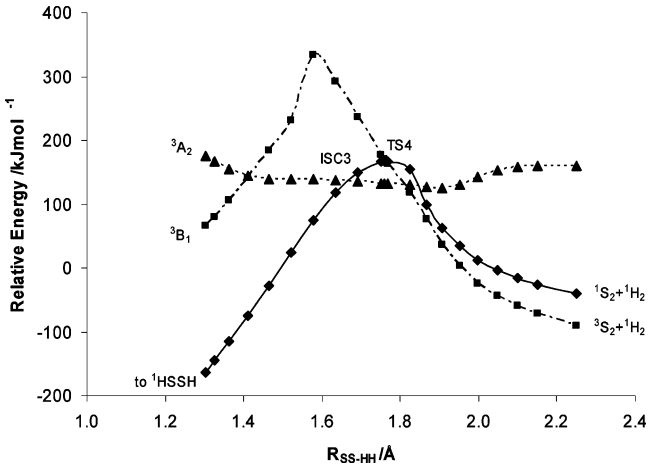

Figure 9. PES of intrinsic reaction coordinate for TS4 with intermediate geometries optimized on singlet surface at MRCI/aug-cc-pVTZ level of theory. One singlet state and two triplet state energies are calculated at MRCI+Davidson/aug-cc-pV(Q+d)Z level and showed relative to SH + SH (excluding ZPVE). R_{SS-HH} represents the distance between the center of two S atoms and that of two H atoms.

and found to have a $^3B_1$ ground state. The trans structure was found to be more stable by 2.3 kJ mol^{-1}; however it is the cis structure that can lead to $H_2 + S_2$. An excited $^3A_2$ *cis*-HSSH isomer was found 109 kJ mol^{-1} above the $^3B_1$ *cis*-isomer. It is relevant to note however that there are somewhat long S−S bonds of ∼2.6 Å in both $^3B_1$ isomers, while that in singlet and $^3A_2$ HSSH is ∼2.0 Å. The intersystem crossing is studied in terms of C_{2v} parallel insertion of S_2 to H_2. Since there is significant variation of sulfur bond length between singlet HSSH (2.0 Å), triplet *cis*-HSSH (2.6 Å), and the transition state TS4 (2.3 Å), plotting a potential energy profile with a constrained sulfur bond is not reasonable. As an alternative, an intrinsic reaction coordinate (IRC) calculation was performed with C_{2v} symmetry on the singlet surface at the MRCI/aug-cc-pVTZ level of theory. Subsequent singlet and triplet energies were calculated at the MRCI/aug-cc-pV(Q+d))Z level, using the geometries optimized in the IRC calculation. Figure 9 shows the multistate PES as a function of distance (R_{SS-HH}) between the center of S_2 and that of H_2. The triplet energy is represented by two triplet states ($^3B_1$ and $^3A_2$) as the triplet ground state changes during the course of the R_{SS-HH} variation. Figure 9 shows there is an intersystem crossing between $^1A_1$ and $^3A_2$ (and a later one from $^3A_2$ to $^3B_1$) before reaching the singlet saddle point on the reactant side, and the contribution of this crossing is to reduce the barrier by ∼22 kJ mol^{-1}. As a consequence, $S_2(^3\Sigma_g^-) + H_2$ is not expected to be produced from HSSH direct dissociation due to a substantial barrier.

3.2. Kinetics. The PES shown in Figure 4 reveals that S insertion and intersystem crossing in R4 is energetically favored over hydrogen abstraction on the triplet surface. This situation is similar to that reported for R3,[11,13,15] with the triplet barrier being even greater with R4a than it is with R3a (19 vs 8 kJ mol^{-1}). Given recent dynamics studies show that one S atom brings 3 times larger spin−orbit coupling than the analogous O system, which in part leads to intersystem crossing,[16] it is sensible to say that there is even stronger spin−orbit coupling in the current two S atoms system so that the kinetics of R4 are indeed dominated by the insertion channel. The intermediate singlet H_2S_2* formed at the crossing point can decompose to form SH + SH, HSS + H, or $S_2 + H_2$, but the formation of HSS + H is 60 kJ mol^{-1} more endothermic than for SH + SH, while formation of $S_2 + H_2$ entails a barrier 21 kJ mol^{-1} above SH + SH. As a consequence, the formation of SH + SH is expected to dominate the product channel via intersystem crossing, except at high pressures when intermediate can be effectively stabilized to H_2SS or more stable HSSH.

The kinetic advantage of the insertion route relative to the abstraction route (due to bypassing the triplet barrier of 19.1 kJ mol^{-1}) will diminish at higher temperatures, especially as the abstraction channel can be expected to have a higher A factor due to the high transition-state entropy change and the avoidance of the intersystem crossing. Figure 10 shows the experimental rate constants reported by Shiina et al.[13] (1050−1540 K) together with the TST abstraction rate on the triplet surface calculated in this work (solid line). Clearly, it is not true to say that R4 is always dominated by intersystem crossing and insertion reaction because the abstraction channel accounts for most if not all of the reaction at the highest temperatures and is never truly negligible even at the lowest temperatures reached in the Shiina study.

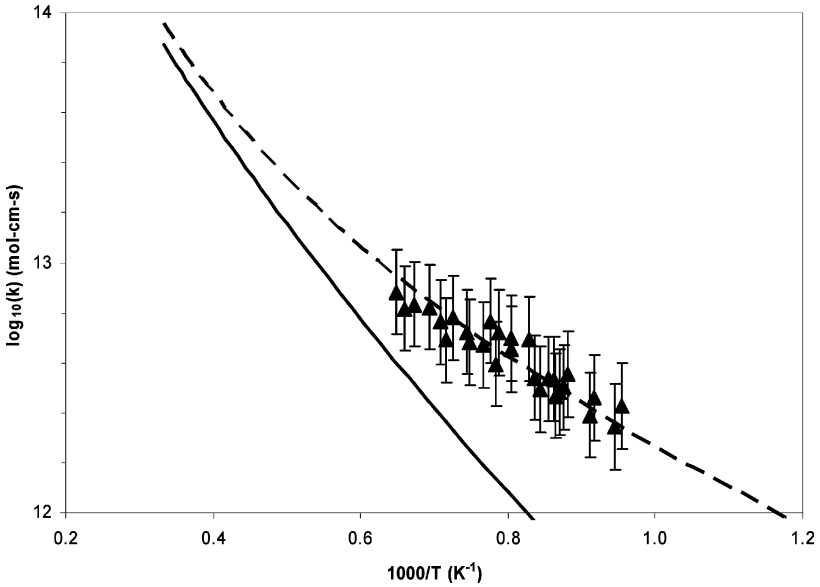

Figure 10. Rate constant of reaction $H_2S + S = SH + SH$. (▲) Measurements by Shiina et al.,[13] solid line represents hydrogen abstraction rate constant derived by TST; broken line represents rate constant derived from a least-squares fit to Shiina's data taking account of both hydrogen abstraction and sulfur insertion.

The dashed line in Figure 10 is a least-squares fit to the data of Shiina et al.,[13] based on additive contributions from abstraction and insertion channels

$$k_{overall} = k_{abs} + k_{ins}$$

The value of k_{abs} is taken as that obtained in this work by TST analysis, but there is no simple means of estimating the rate of intersystem crossing. Therefore, we estimate k_{ins} from the data fit to $k_{overall}$, assuming that the activation energy for the insertion channel is equal to the endothermicity of R4a,b. This analysis yields the Arrhenius expression for the insertion rate

$$k_{ins} = 3.7 \times 10^{13} \exp(-26.2 \text{ kJ mol}^{-1}/RT) \text{ cm}^3 \text{ mol}^{-1} \text{ s}^{-1}$$

The A factor of 3.7×10^{13} cm^3 mol^{-1} s^{-1} for the insertion channel seems at first sight to be high for a system-crossing reaction. However, we note that this A factor is significantly smaller than the value of 6.9×10^{14} cm^3 mol^{-1} s^{-1} corresponding to a two-parameter Arrhenius fit for the abstraction channel (for which $E_a = 65$ kJ mol^{-1}). We can also compare the A factor for the insertion channel R4b with that for reaction R3 (1.4×10^{14} cm^3 mol^{-1} s^{-1})[15] for which the insertion channel is also energetically preferred; however this comparison should be treated with care as there may be some contribution from the abstraction channel in R3 at high temperatures, just as appears to be the case for R4(a+b).

4. Conclusions

The PES for the H_2/S_2 system characterized at the MRCI level indicates the presence of an intersystem crossing which effectively offers a channel without barrier for the reverse reaction of $H_2S + S \rightarrow SH + SH$. Once on the singlet surface, other channels are also accessible in this system, including the formation of HSS + H and $S_2 + H_2$, but these are energetically unfavorable with respect to SH + SH by 60 kJ mol^{-1} (product energy) and 21 kJ mol^{-1} (transition state barrier), respectively. Additional intersystem crossings are also possible, but these are not expected to influence the product distribution of the H_2S + S reaction.

While the insertion channel with intersystem crossing bypasses the 19.1 kJ mol^{-1} of the triplet abstraction barrier, the abstraction channel must have a higher Arrhenius factor and therefore becomes competitive at higher temperatures. Comparison of experimental data for the rate of reaction of H_2S + S ($1050 < T$ (K) < 1540) with a TST calculation of the rate constant for the abstraction channel confirms that this channel plays a significant role in the formation of products, especially at the higher temperatures. However the abstraction channel cannot account for all of the experimentally observed rate, especially at the lower temperatures, and it is possible to estimate the rate of the reaction via what is presumably the insertion channel. This channel has no significant barrier (beyond the 26.2 kJ mol^{-1} overall endothermicity) and has a somewhat smaller Arrhenius pre-exponential factor than the abstraction route.

It is concluded that the reaction $H_2S + S \rightarrow SH + SH$ is energetically favored, by 19.1 kJ mol^{-1}, through triplet-singlet intersystem crossing and insertion. This will be the dominant channel for reaction at sufficiently low temperature, but the abstraction channel becomes important at higher temperatures. We expect the same phenomena to arise in the $H_2 + S \rightarrow SH + H$ reaction, which is also believed to be energetically favorable (by just 8 kJ mol^{-1}) when proceeding via intersystem crossing and insertion. Extrapolation of experimental results to higher or lower temperatures should be undertaken with great care with such reactions.

Acknowledgment. The authors acknowledge the support of the Australian Research Council for part of this work. The computations were performed at Australia Partnership for Advanced Computing at the Australian National University, Canberra. Chenlai (Ryan) Zhou thanks the School of Chemical and Biomolecular Engineering of the University of Sydney for the award of the FH Loxton Postgraduate Studentship.

Supporting Information Available: Geometries of all species and transition states presented. This material is available free of charge via the Internet at http://pubs.acs.org.

References and Notes

(1) Schofield, K. *Combust. Flame* **2001**, *124*, 137.
(2) Darwent, B. D.; Roberts, R. *Proc. R. Soc. London, Ser. A* **1953**, *216*, 344.
(3) Kaloidas, V.; Papayannakos, N. *Chem. Eng. Sci.* **1989**, *44*, 2493.
(4) Tesner, P. A.; Nemirovskii, M. S.; Motyl, D. N. *Kinet. Catal.* **1990**, *31*, 1081.
(5) Adesina, A. A.; Meeyoo, V.; Foulds, G. *Int. J. Hydrogen Energ.* **1995**, *20*, 777.
(6) Hawboldt, K. A.; Monnery, W. D.; Svrcek, W. Y. *Chem. Eng. Sci.* **2000**, *55*, 957.
(7) Binoist, M.; Labegorre, B.; Monnet, F.; Clark, P. D.; Dowling, N. I.; Huang, M.; Archambault, D.; Plasari, E.; Marquaire, P. M. *Ind. Eng. Chem. Res.* **2003**, *42*, 3943.
(8) Higashihara, T.; Saito, K.; Yamamura, H. *B. Chem. Soc. Jpn.* **1976**, *49*, 965.
(9) Bowman, C. T.; Dodge, L. G. *Proc. Combust. Inst.* **1976**, *16*, 971.
(10) Roth, P.; Lohr, R.; Barner, U. *Combust. Flame* **1982**, *45*, 273.
(11) Woiki, D.; Roth, P. *J. Phys. Chem.* **1994**, *98*, 12958.
(12) Olschewski, H. A.; Troe, J.; Wagner, H. G. *J. Phys. Chem.* **1994**, *98*, 12964.
(13) Shiina, H.; Oya, M.; Yamashita, K.; Miyoshi, A.; Matsui, H. *J. Phys. Chem.* **1996**, *100*, 2136.
(14) Sendt, K.; Jazbec, M.; Haynes, B. S. *Proc. Combust. Inst.* **2003**, *29*, 2439.
(15) Shiina, H.; Miyoshi, A.; Matsui, H. *J. Phys. Chem. A* **1998**, *102*, 3556.
(16) Maiti, B.; Schatz, G. C.; Lendvay, G. *J. Phys. Chem. A* **2004**, *108*, 8772.
(17) Tsuchiya, K.; Yamashita, K.; Miyoshi, A.; Matsui, H. *J. Phys. Chem.* **1996**, *100*, 17202.
(18) Langhoff, S. R.; Davidson, E. R. *Int. J. Quantum Chem.* **1974**, *8*, 61.
(19) Dunning, T. H.; Peterson, K. A.; Wilson, A. K. *J. Chem. Phys.* **2001**, *114*, 9244.
(20) Sendt, K.; Haynes, B. S. *Proc. Combust. Inst.* **2007**, *31*, 257.
(21) Werner, H.-J.; Lindh, P. J. K.; Manby, R. F. R.; Schütz, M. *MOLPRO, version 2006.1, a package of ab initio programs*.
(22) Helgaker, T.; Jensen, H. J.; Joergensen, P.; Olsen, J. *Dalton Release 1.1 (2000), an electronic structure program*; 2000.
(23) Frisch, M. J.; Trucks, G. W.; Schlegel, H. B.; Scuseria, G. E.; Robb, M. A.; Cheeseman, J. R.; Zakrzewski, V. G.; Montgomery, J. A. Jr.; Stratmann, R. E.; Burant, J. C.; Dapprich, S.; Millam, J. M.; Daniels, A. D.; Kudin, K. N.; Strain, M. C.; Farkas, O.; Tomasi, J.; Barone, V.; Cossi, M.; Cammi, R.; Mennucci, B.; Pomelli, C.; Adamo, C.; Clifford, S.; Ochterski, J.; Petersson, G. A.; Ayala, P. Y.; Cui, Q.; Morokuma, K.; Malick, D. K.; Rabuck, A. D.; Raghavachari, K.; Foresman, J. B.; Cioslowski, J.; Ortiz, J. V.; Stefanov, B. B.; Liu, G.; Liashenko, A.; Piskorz, P.; Komaromi, I.; Gomperts, R.; Martin, R. L.; Fox, D. J.; Keith, T.; Al-Laham, M. A.; Peng, C. Y.; Nanayakkara, A.; Gonzalez, C.; Challacombe, M.; Gill, P. M. W.; Johnson, B. G.; Chen, W.; Wong, M. W.; Andres, J. L.; Head-Gordon, M.; Replogle, E. S.; Pople, J. A. *Gaussian 98*, revision A.9; Gaussian, Inc.: Pittsburgh, PA, 1998.
(24) Wigner, E. P. Z. *Phys. Chem. B* **1932**, *19*, 203.
(25) Steudel, R.; Drozdova, Y.; Miaskiewicz, K.; Hertwig, R. H.; Koch, W. *J. Am. Chem. Soc.* **1997**, *119*, 1990.
(26) Benson, S. W. *Chem. Rev.* **1978**, *78*, 23.
(27) Steudel, R.; Steudel, Y.; Miaskiewicz, K. *Chem.−Eur. J.* **2001**, *7*, 3281.

(28) Shiell, R. C.; Hu, X. K.; Hu, Q. J.; Hepburn, J. W. *J. Phys. Chem. A* **2000**, *104*, 4339.
(29) Chase, M. W. NIST-JANAF Thermochemical Tables Fourth Edition. *J. Phys. Chem. Ref. Data* **1998**, Monograph No. 9.
(30) Decker, B. K.; Adams, N. G.; Babcock, L. M.; Crawford, T. D.; Schaefer, H. F. *J. Phys. Chem. A* **2000**, *104*, 4636.
(31) Behrend, J.; Mittler, P.; Winnewisser, G.; Yamada, K. M. T. *J. Mol. Spectrosc.* **1991**, *150*, 99.
(32) Huber, K. P.; Herzberg, G. *Van Nostrand Reinhold Co.* **1979**.
(33) Herzberg, G. *Van Nostrand*; New York, 1966.
(34) Tanimoto, M.; Klaus, T.; Muller, H. S. P.; Winnewisser, G. *J. Mol. Spectrosc.* **2000**, *199*, 73.